Journal of Orthopaedic Translation 48 (2024) 11–24

Contents lists available at ScienceDirect

Journal of Orthopaedic Translation

journal homepage: www.journals.elsevier.com/journal-of-orthopaedic-translation

Original Article

Hyperbaric oxygen promotes bone regeneration by activating the mechanosensitive Piezo1 pathway in osteogenic progenitors

Hang Zhou [a,b], Hongzhi Liu [a,b], Minmin Lin [a,b], Hantang Wang [a,b], Jingjing Zhou [a,b], Ming Li [c], Xue Yang [c,**], Guibing Fu [d,***], Chao Liu [a,b,*]

[a] Department of Biomedical Engineering, College of Engineering, Southern University of Science and Technology, Engineering Building south 622, 1088 Xueyuan Avenue, Shenzhen, Guangdong, China
[b] Guangdong Provincial Key Laboratory of Advanced Biomaterials, Southern University of Science and Technology, Engineering Building south 622, 1088 Xueyuan Avenue, Shenzhen, Guangdong, China
[c] Department of Rehabilitation Medicine, Shenzhen Children's Hospital, No. 7019 Yitian Road, Futian District, Shenzhen, Guangdong, China
[d] Department of Pediatric Orthopedics, Shenzhen Children's Hospital, No. 7019 Yitian Road, Futian District, Shenzhen, Guangdong, China

ARTICLE INFO

Keywords:
Angiogenesis
Bone regeneration
Hyperbaric oxygenation
Osteogenesis
Piezo1
YAP

ABSTRACT

Background: Hyperbaric oxygen (HBO) therapy is widely used to treat bone defects, but the correlation of high oxygen concentration and pressure to osteogenesis is unclear.
Methods: Bilateral monocortical tibial defect surgeries were performed on 12-week-old Prrx1-Cre; Rosa26-tdTomato and Prrx1-Cre; Piezo1$^{fl/+}$ mice. Daily HBO treatment was applied on post-surgery day (PSD) 1–9; and daily mechanical loading on tibia was from PSD 5 to 8. The mice were euthanized on PSD 10, and bone defect repair in their tibias was evaluated using μCT, biomechanical testing, and immunofluorescence deep-tissue imaging. The degree of angiogenesis–osteogenesis coupling was determined through spatial correlation analysis. Bone marrow stromal cells from knockout mice were cultured in vitro, and their osteogenic capacities of the cells were assessed. The activation of genes in the Piezo1–YAP pathway was evaluated using RNA sequencing and quantitative real-time polymerase chain reaction.
Results: Lineage tracing showed HBO therapy considerably altered the number of Prrx1^{+} cells and their progeny in a healing bone defect. Using conditional knockdown mice, we found that HBO stimulation activates the Piezo1–YAP axis in Prrx1^{+} cells and promotes osteogenesis–angiogenesis coupling during bone repair. The beneficial effect of HBO was similar to that of anabolic mechanical stimulation, which also acts through the Piezo1–YAP axis. Subsequent transcriptome sequencing results revealed that similar mechanosensitive pathways are activated by HBO therapy in a bone defect.
Conclusion: HBO therapy promotes bone tissue regeneration through the mechanosensitive Piezo1–YAP pathway in a population of Prrx1^{+} osteogenic progenitors. Our results contribute to the understanding of the mechanism by which HBO therapy treats bone defects.
The Translational Potential of this Article: Hyperbaric oxygen therapy is widely used in clinical settings. Our results show that osteogenesis was induced by the activation of the Piezo1–YAP pathway in osteoprogenitors after HBO stimulation, and the underlying mechanism was elucidated. These results may help improve current HBO methods and lead to the formulation of alternative treatments that achieve the same functional outcomes.

1. Introduction

Hyperbaric oxygen (HBO) therapy refers to a treatment using pure oxygen at pressure higher than one atmosphere. HBO has been integrated with clinical treatments for nearly a hundred diseases, such as cardiopulmonary resuscitation, neurological diseases, cardiovascular

* Corresponding author. Department of Biomedical Engineering, College of Engineering, Southern University of Science and Technology, Engineering Building south 622, 1088 Xueyuan Avenue, Shenzhen, Guangdong, China.
** Corresponding author.
*** Corresponding author.
E-mail addresses: snowyang5@126.com (X. Yang), fgbmd@163.com (G. Fu), liuc33@sustech.edu.cn (C. Liu).

https://doi.org/10.1016/j.jot.2024.07.001
Received 3 April 2024; Received in revised form 17 June 2024; Accepted 3 July 2024

diseases, and gas embolism [1–3]. HBO increases oxygen penetration and the amount of dissolved oxygen in the blood and tissues. HBO therapy exhibits significant effect in reducing inflammation [4]. HBO therapy has also shown efficacy for tissue regeneration, such as skin and bone tissue regeneration [5–9]. However, the biological mechanisms during the treatment process are still unclear.

Fractures reduce quality of life, increase mortality, and impose considerable economic burden [10]. The extended length of time for a bone defect to heal is long, imposes financial burden, induces comorbidities, and increases mortality. Some bone defects do not heal, increasing personal and societal costs. Bone tissue regeneration is sensitive to mechanical forces. Mechanical loading during the matrix deposition phase enhances bone repair [11–14]. In mice, bone repair depends on angiogenesis because the enhancement of angiogenesis accelerates fracture healing [15–19]. For example, cilostazol can stimulate angiogenesis and promote bone repair [20]. Conversely, the inhibition of angiogenesis completely abolishes new bone formation in rats with bone fracture [21]. Type H vessels are present during bone formation [22,23], showing high levels of CD31 and EMCN expression and playing an important role in bone tissue regeneration [24]. These unique vessels could be upregulated by mechanical loading and led to an increase in bone mass through angiogenesis–osteogenesis coupling [25,26].

Skeletal stem cells expressing Prrx1 would migrate into bone defects and undergo osteogenic differentiation. Prrx1^{+} cells and their derivatives, which are called osteogenic progenitors, are required for homeostasis and repair of trabecular and endosteal bones in adult mice [27–30]. The depletion of Prrx1^{+} cells would result in compromised fracture healing [31]. Osteogenic progenitors are mechanosensitive cells regulated by mechanical signals during bone fracture repair [32]. Piezo1, a major membrane mechanosensory protein, is regarded as a major mechanosensor in bone homeostasis, while conditional knockout of Piezo1 in Prrx1^{+} cells resulted in severe bone developmental defects [33–36]. Piezo1/YAP/Runx2 is one of important signaling pathways for osteogenesis [37,38].

HBO stimulates through hyperphysiological oxygen concentration and high pressure. As Piezo1 could be modulated by oxygen [39] and mechanical forces [33,34], we speculated that HBO activates Piezo1 and related signaling pathway in osteogenic cells to promote bone regeneration.

In this study, we hypothesized that HBO promotes bone regeneration by activating the mechanosensitive pathways in osteogenic progenitors though the Piezo1–YAP axis. We used a tibial defect bone repair model, which produces a consistent repair response in time and space [12], and a three-dimensional (3D) high-resolution imaging platform to observe and quantify vessels and osteogenic progenitors during bone repair. We found that HBO therapy promoted bone repair by promoting angiogenesis and osteogenesis. HBO activated the expression of Piezo1 and downstream genes in the Prrx1^{+} cells, and the conditional knockout of Piezo1 expression inhibited the pro-osteogenic effects of HBO and mechanical loading.

2. Materials and methods

2.1. Animals

All the animals in this study were mice of C57BL/6J background. All the mice were housed under specific pathogen-free (SPF) conditions in the Southern University of Science and Technology Animal Care Facility and had access ad libitum to standard mouse chow and water for the duration of the study. Twelve-week-old female mice were used for in vivo surgery and bone analysis regardless of their genotype. C57BL/6J mice were used for all wild-type (WT) bone analysis. Mice with conditionally knocked out Piezo1 expression in Prrx1^{+} cells (Prrx1–Cre, Piezo1$^{flox/flox}$ and Prrx1-Cre, Piezo1$^{flox/+}$) were obtained by crossing the Prrx1–Cre mice and Piezo1$^{flox/flox}$ mice. Mice with tracked Prrx1^{+} cells by tdTomato (Prrx1–Cre, tdTomato) were obtained by crossing the Prrx1–Cre mice and Ai14(RCL-tdT)-D mice. The Ai14(RCL-tdT)-D mice were purchased from the Jackson laboratory. The Prrx1–Cre mice and Piezo1$^{flox/flox}$ mice were purchased from Cyagen Biosciences. All in vivo animal protocols were approved by the Institutional Animal Care and Use Committee (SUSTech-JY202201011). Before sample collection, mice were anesthetized with isoflurane (2 % in air) and euthanized by cervical dislocation.

2.2. Long-bone defect repair model

Mouse monocortical tibia defect (MTD) surgery was conducted as previously described [12]. All the mice were anesthetized with isoflurane (1.5 % in air), and subcutaneous meloxicam was used as analgesic (1 mg/kg). We first made a longitudinal skin incision over the lower limb. Then, we created a 1 mm-diameter circular defect with a high-speed drill on the anterior medial surface of the mouse tibia centered between the tibiofibular junction and tibial tubercle. The defect center was 4 mm distal to the proximal articulating surfacing of the tibia. The incision was closed with 6-0 nylon sutures after saline irrigation. A heating pad was used to protect mice from hypothermia. Erythromycin ointment was used after the surgery to protect the wound from infection.

2.3. HBO treatment

Mice in the HBO group were placed in the hyperbaric oxygen chamber. We first increased the oxygen concentration to 95 % in the chamber. Then the pressure was increased to 2.4 atm absolute (ATA) with the duration of 14 min, while the oxygen concentration was further increased to 98 %. Mice remained in this hyperbaric oxygen environment for 90 min, then removed after 14 min of decompression. The treatment was performed once a day after the surgery. Mice showed no obvious pain or discomfort during hyperbaric oxygen treatment.

2.4. Mechanical loading

Mice were anesthetized with isoflurane (1.5 % in air). The left tibia was axially compressed by an electromagnetic mechanical test system (M−100, CARE Measurement & Control, Tianjin, China). Loading was applied once a day on PSD 5–8, using a continuous sinusoidal waveform at 2 Hz, with a force amplitude of 1–6 N for 120 cycles. The right tibiae were not loaded, serving as contralateral control. Mice showed no obvious pain or discomfort during mechanical loading.

2.5. Microcomputed tomography

The tibias were harvested, and scanned using a microcomputed tomography (micro-CT) scanner (Skyscan 1172, Bruker, USA) at a voltage of 60 kV, current of 100 μA, and resolution of 6 μm. The CTAn software was used to analyze bone volume to total volume (BV/TV) ratio, trabecular number (Tb.N), trabecular thickness (Tb.Th), and trabecular spacing (Tb.Sp). The 3D reconstruction of the intact bone and defect region was performed using CTvox (Bruker, USA). The volume of interest (VOI) was the circular region of the tibial defect, on the same frontal plane as the existing cortical bone. BV/TV was defined as the ratio of the segmented bone volume to the total volume in the VOI. Tb.N, Th.Th, and Tb.Sp were defined as the average number of trabeculae per unit length, mean thickness of trabeculae, and distance between trabeculae in the VOI, respectively. The computation of Tb.N, Th.Th, and Tb.Sp was based on 3D calculations, namely, a sphere fitting method [40]. The basic approach is to determine the diameter of the largest possible sphere that can be fitted through each voxel that is completely contained within an object (or background) and then to average these diameters.

2.6. Mechanical testing

The mechanical properties of the bone-defect tissue were determined using digital image correlation (DIC) according to previously published methods [41]. The surfaces of the tibias were coated with a layer of matt and water-based white acrylic paint (XF-2, Tamiya Paint, USA) and then speckled with matt and water-based black paint (0741, Haoshun, China) with a high-precision airbrush. The painted tibias were placed in the loading cups of an electromagnetic mechanical test system (M−100, CARE Measurement & Control, Tianjin, China). Axial compressive mechanical load was applied at a rate of 8 N/min up to a maximum of 12 N, and the strain field was determined using the 3D DIC system (XTDIC--Micro, XTOP, China).

2.7. Immunofluorescent staining of thick bone sections

Mice were sacrificed on PSD 4 and 8. Frozen thick longitudinal tibia sections (80 μm) were prepared as described previously [42]. Soft tissues were stripped off from each tibia, which was fixed in 4 % paraformaldehyde (PFA) at 4 °C for 4 h, decalcified in 0.5 M EDTA at 4 °C for 24 h, cryoprotected at 4 °C for 24 h, and cryoembedded. Cryosections were prepared using a cryostat (Leica 3050S) with a thickness of 80 μm and stored at −80 °C.

For immunostaining, the tibia sections were hydrated, permeabilized, blocked, and incubated with primary antibodies against endomucin (V.7C7, 1:200, SANTACRUZ), Prrx1 (ab211292, 1:200, Abcam), CD31 (FAB3628G, 1:200, R&D), and YAP (14074S, 1:200, Cell Signaling Technology) overnight. The next day, the sections were incubated with antirabbit Alexa Fluor 647 (A31573, 1:300, Thermo Fisher) or antigoat Alexa Fluor 647 (A21247, 1:300, Thermo Fisher) secondary antibody for 1 h at room temperature. The sections were washed with phosphate-buffered saline (PBS), mounted with DAPI FluoroMount-G (0100-20, SouthernBiotech), and sealed with coverslips.

2.8. Confocal and two-photon imaging

A Zeiss LSM980 confocal laser scanning microscope with a 20 × objective lens was used in obtaining 3D fluorescent images. The z stacks of 40 μm in height and an x-y detect area at a size of 1024 × 1024 pixels, with a resolution of 0.414 μm, were taken for each slide, and a 1-mm defect was imaged by tiling four z stacks, spanning 1600 mm along the long axis of the tibia.

The second harmonic generation of collagen fibers was acquired using an Olympus FVMPE-RS Multiphoton laser scanning microscope (Japan). Images were excited with an 860 nm laser, and emissions were detected using 420–465 filters. The z stack of 40 μm height and an x-y detect area, at a size of 1024 × 1024 pixels, with a resolution of 0.414 μm, were obtained from each sample.

2.9. 3D image analysis

The z stacks obtained from two-photon microscopy were rendered in 3D using Bitplane Imaris v7.4.1 and Fiji. In the deep-tissue images of longitudinal thick sections of the MTD, the irregular VOIs of the whole bone defect were selected as quantitative regions, including cortical bone and bone marrow defects. These VOIs were used for the analysis of the effects of HBO therapy and mechanical loading on multiple tissue types and progenitor cell populations within a healing defect. 3D volumes generated from the VOIs were used in the segmentation and quantification of type H vessels ($EMCN^+CD31^+$), skeletal stem cells ($Prrx1^+$), and several proteins in osteogenic progenitors (Piezo1, YAP, Runx2). Cells with nuclear staining (Prrx1, YAP, Runx2) that have fluorescence signal overlaps due to proximity were segmented using the watershed method [43], which effectively separated individual cells and identified objects with size of 5 microns. A similar method was used for the quantification of cells with membrane staining (Piezo1), and a seven-micron cutoff for watershed segmentation was used. Cells co-expressing Prrx1, YAP, and DAPI were identified when a positive fluorescence signal from corresponding channels was observed. The location, sizes, surface areas, and volumes of cells were computed by generating 3D-rendered surfaces from immunofluorescence and colocalization data. Surfaces were generated for vascular structure, but individual endothelial cells were not segmented. Bone tissue was segmented by thresholding the second harmonic generation data with the same algorithm as that used for vessels.

2.10. Spatiotemporal analysis of osteogenic progenitors and type H vessels

The 3D surfaces of each confocal channel were created by utilizing the surface function in Imaris (v.7.1, Oxford Instruments, Switzerland). The spatial positions of cells (Prrx1, DAPI) were obtained by the position output in Imaris and saved as excel files. The distance distribution to selected surfaces (EMCN, CD31) was generated using the Distance Transformation tool in Imaris and saved as TIFF files. For cell-to-surface analysis, the position information of $Prrx1^+$ cells and the distance distribution to surface were input into MATLAB script. The distance distribution of $Prrx1^+$ cells versus vessels was analyzed by utilizing cell-to-surface code (cell-to-surface code.m).

2.11. Histological staining

The tibias with MTD were extracted on PSD 10, fixed in 4 % PFA for 24 h, and decalcified in a large volume of 0.5 M EDTA at 4 °C for 3 weeks before tissue processing. Then, tissue samples were dehydrated, embedded in paraffin (Leica ASP 300S, Leica), and 8 μm-thick paraffin sections were created using a microtome (Leica CM1950, Leica) and stained with hematoxylin and eosin (H&E; G1120, Solarbio, China) and Goldner's trichrome staining (G1064, Servicebio, China) according to the manufacturers' instructions.

2.12. qRT-PCR

A 3 mm-thick section of tibia containing the defect was collected on PSD 8 and ground into powder at −80 °C with TissueLyser (Jingxin, China). Total RNA was extracted using TRIzol (15596, Thermo Scientific, USA). A RevertAid First Strand cDNA Synthesis Kit (K1622, Thermo Fisher Scientific, USA) was utilized for the synthesis of cDNA from isolated total RNA. The relative expression levels of osteogenic- and angiogenic-related genes in the defects were assessed by quantitative real-time polymerase chain reaction (qRT-PCR) using GoTaq qPCR Master Mix (A6002, Promega, USA). Primer sequences are listed in Table S1, and gene expression was presented as $2^{-(\Delta\Delta CT)}$ after normalization to 18 s.

2.13. Bone marrow stromal cells isolation and culture

Bone marrow stromal cells (BMSCs) were isolated from the femurs and tibias of six-week-old female C57BL/6J mice according to previously published methods [44]. The bone marrow of female C57BL/6 mice was extracted by rinsing the bone cavities with culture medium (αMEM + 1 % P/S + 10 % FBS). Nonadherent cells were removed by replacing the medium and washing with PBS. The extracted BMSCs (2×10^6 cells) were cultured in a 25 cm^2 cell culture flask at 37 °C in an atmosphere of 5 % carbon dioxide.

2.14. BMSCs treatment

BMSCs were cultured in a six-well plate (TCP010006, JETBIOFIL), with a density of 5×10^5 cells per well. For BMSCs in fluid shear stress (FSS) group, 0.85 Pa of FSS was applied for 2 h with an orbital shaker. For BMSCs in HBO group, we placed the six-well plate in the HBO chamber and increased the oxygen concentration to 95 % in the

chamber. Then the pressure was increased to 1.8 ATA with the duration of 5 min. BMSCs remained in this hyperbaric oxygen environment for 20 min, then removed after 5 min of decompression. The culture medium was replenished every 2 days.

2.15. Alizarin red staining

BMSCs were incubated with indicated interventions in an osteogenic medium containing a growth medium supplemented with β-glycerophosphate (10 mM), dexamethasone (100 nM), and ascorbic acid (50 μg/mL) for 21 days. The medium was changed every 3 days. On day 21, the BMSCs were washed three times with PBS and fixed for 20 min in 4 % paraformaldehyde and washed twice and incubated with 0.2 % alizarin red solution (C0148S, Beyotime, China, pH 4.2) for 20 min. Excessive dye was removed by washing with distilled water. Alizarin red staining was examined and photographed with microscope.

2.16. Alkaline phosphatase staining

Alkaline phosphatase (ALP) staining for ALP formation was performed by using a BCIP/NBT alkaline phosphatase color development kit (P0321S, Beyotime, China). Briefly, the BMSCs were washed three times with PBS and fixed for 20 min in 4 % paraformaldehyde and washed twice and incubated with alkaline phosphatase color solution for 30 min. Excessive dye was removed by washing with distilled water. VICs were examined and photographed with microscope.

2.17. Calcium imaging

BMSCs were washed three times with PBS and then incubated with 2 μM Fluo-4 AM (F14201, Thermo Fisher) for 10 min at 37 °C in 5 % CO^2. Ca^{2+} fluorescence intensity was captured at a scan time of 470 ms per frame for 3 min with a confocal microscope (Zeiss LSM980). During the

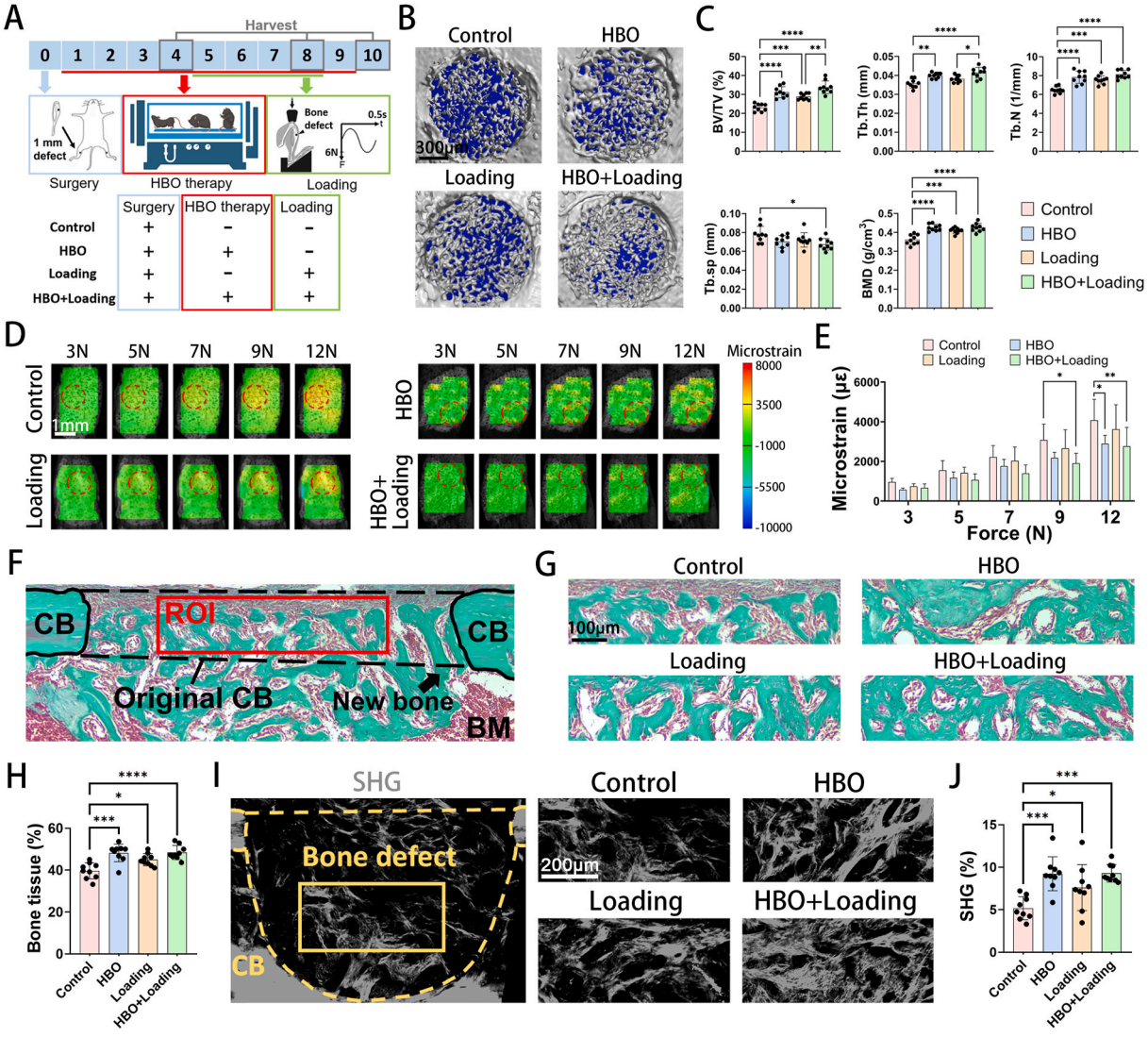

Fig. 1. HBO therapy and mechanical loading increased bone volume and strength in bone defects. (A) Schematic illustration of the design of animal experiments to test the effect of HBO therapy and mechanical loading on bone repair. (**B**) Micro-CT reconstruction of cortical bone defects on PSD10. (**C**) Bone morphometric properties and bone mineral density (BMD) of bone defect regions on PSD10; n = 9. (**D**) DIC measurement of strain at tibia surface with defects under 3–12 N of axial loading; red dotted line indicates defect region. (**E**) Maximum strain over the defect caused by axial loading; n = 6. (**F–G**) Goldner's trichrome staining of cortical bone defect region (**F**). CB, cortical bone; BM, bone marrow; zoomed-in images of regions (**G**) enclosed by red lines are shown below. (**H**) Bone tissue area from Goldner's trichrome staining, the whole original CB region analyzed; n = 6. (**I**) SHG signals from collagen fibers in the cortical bone defect region on PSD8. CB, cortical bone; zoomed-in images of regions enclosed by yellow lines are shown right. (**J**) Volume of SHG on PSD8; the whole bone defect region enclosed by yellow dotted lines analyzed; n = 6. Data are means ± SD. *p < 0.05, **p < 0.01, ***p < 0.001, ****p < 0.0001. (For interpretation of the references to color in this figure legend, the reader is referred to the Web version of this article.)

experiment, 10 μM Yoda1 (SML1558, Sigma–Aldrich) was added in the Yoda1 group to activate Piezo1.

2.18. Statistical analysis

Statistical significance between two groups were evaluated with Student's t-test. Multiple-group comparison was performed with one-way and two-way ANOVA tests with Tukey's multiple-comparison test. Experimental data were expressed as means ± SD. Results were considered statistically significant if $p < 0.05$. GraphPad 9.0 software (GraphPad Software, La Jolla, CA, USA) was used for all statistical analyses.

3. Results

3.1. HBO therapy promotes bone repair with similar effectiveness as mechanical loading

To analyze the effect of HBO therapy and mechanical loading on bone tissue regeneration, we conducted mouse MTD surgery and assessed bone tissue regeneration by micro-CT, DIC and histological staining (Fig. 1A). On PSD 10, when the bone mass in the bone defect reached its peak, micro-CT data showed that HBO therapy significantly promoted the repair of cortical bone in the bone defect, with an effect similar to that of mechanical loading (Fig. 1B). BV/TV, Tb.Th, Tb.N, and bone mineral density (BMD) in the HBO group were significantly higher than those in the control group. When mechanical loading was combined with HBO therapy, no significant improvement in bone defect repair was observed, compared with that in the single-HBO group (Fig. 1C).

DIC results showed that the bone defect area of the mouse tibia in the HBO group had lower strain under the same intensity of mechanical stimulation, demonstrating that HBO treatment significantly increased the mechanical strength of bone defects. Similarly, when mechanical loading was combined with HBO therapy, the mechanical properties of the bone defects did not show further improvement compared to single-HBO group (Fig. 1D and E). The Goldner's trichrome staining results showed that the area of green bone tissues indicated that both treatments promoted new bone remodeling, consistent with the micro-CT results (Fig. 1F–H). In the treated groups, H&E staining showed increase in newly formed bone in both cortical bone and bone marrow defects (Fig. S1). To analyze collagen in the bone defects, we quantified the results of second harmonic generation (SHG) imaging by building a 3D model [45]. The proportion of collagen in the total bone defect volume showed the positive effect of HBO on bone tissue regeneration (Fig. 1I and J).

3.2. HBO therapy promotes osteogenesis–angiogenesis coupling similar to mechanical loading

In bone defects, newly formed type H vessels ($EMCN^{hi}CD31^{hi}$ cells) are necessary for bone tissue regeneration [22]. To explore how HBO therapy affects the niche and promotes bone tissue regeneration, a confocal imaging and assessment on the whole bone defect area was performed. MTD surgery was conducted on Prrx1-Cre, tdTomato mouse to track osteogenic progenitors during bone repair. Prrx1 is expressed from developmental stages of osteogenic progenitors, and tomato fluorescence is used to track $Prrx1^{+}$ cells and all their derivatives, which are osteogenic progenitors [27]. During the early stage of bone repair, the majority of cells migrating to bone defect are stem cells rather than mature cells. Therefore, tracking osteogenic progenitors can reflect the capacity of stem cell recruitment. On PSD4, when vessels began to invade the bone defect, immunofluorescence showed significantly increased type H vessel volume and osteogenic progenitors in the HBO group. Furthermore, osteogenic progenitors which were closest to type H vessels (distance < 5 μm) were more abundant in the HBO group than the other groups, indicating the positive effect of HBO therapy on angiogenesis and stem cell recruitment (Fig. 2A and B).

It has been reported that mechanical loading during the late stage of regeneration enhances bone repair. Thus, we established a mechanical loading group from PSD5 to PSD8 [12]. On PSD8, when the vessels had filled the bone defect area, stopped invading, and entered the peak stage of osteogenesis, mechanical loading promoted stem cell recruitment, as it has been reported (Fig. 2C and D). HBO therapy showed the same tendency to promote angiogenesis and stem cell recruitment as that observed on PSD4. When HBO therapy was combined with mechanical loading, the promotion on stem cell recruitment was significantly better than that in the single-HBO treatment group, whereas the promotion on angiogenesis did not show a significant increase compared with that in the single-HBO group. These results demonstrated that HBO therapy promotes osteogenesis–angiogenesis coupling during bone tissue regeneration.

3.3. HBO therapy activated the Piezo1–YAP axis in the bone defect tissue

To explore how HBO therapy promotes bone tissue regeneration further, we performed RNA sequencing (RNA-seq) on bone defects on PSD8 (Fig. 3A and B). Interestingly, mechanosensitive pathways were stimulated by HBO therapy according to Gene Ontology (GO) enrichment analysis (Fig. 3C and S2). These pathways have been reported to be stimulated by mechanical loading [37,38,46,47]. The real-time quantitative PCR (qRT-PCR) of bone defects on PSD8 indicated that Piezo1 and YAP, which are important mechanosensitive genes, were upregulated by HBO therapy and mechanical loading. Runx2 and Col1, its downstream osteogenesis-related genes, were also up-regulated (Fig. 3D).

The nuclear localization of YAP protein can activate downstream signaling pathways that promote osteogenesis [38,48]. Immunofluorescence imaging data showed an upward trend in the proportion of osteogenic progenitors with nuclear-localized YAP (Fig. 3E–G). Meanwhile, the nuclear localization rate of YAP was upregulated by both HBO therapy and mechanical loading (Fig. 3H).

3.4. HBO treatment in vitro activated Piezo1–YAP pathway and promoted osteogenesis in $Prrx1^{+}$ cells

To validate the influence of HBO and mechanical loading on mechanosensitive protein, we conducted an in vitro study using BMSCs from Prrx1-Cre, tdTomato mouse femurs and tibias (Fig. 4A). We verified through fluorescence tracking that the proportion of osteogenic progenitors in the total extracted BMSCs was greater than 96 % (Fig. S3). FSS is the dominant mode of mechanical stimulation felt by cells during bone regeneration [49,50]. We applied oscillatory laminar flow to stimulate BMSCs during osteogenic differentiation.

Immunofluorescence data showed that after 7 and 14 days of osteogenic induction, the volume of Piezo1 was significantly upregulated by HBO + FSS treatment, which is consistent with our in vivo findings (Fig. 4B–D). Another mechanosensitive marker, YAP, which is a downstream mechanosensor of Piezo1, showed a significantly more pronounced nuclear localization in the HBO and HBO + FSS groups (Fig. 4E and F). The results of assessment of YAP nuclear translocation confirmed this observation (Fig. 4G).

To determine whether the increase in mechanosensitive proteins caused by HBO and FSS can promote osteogenesis, we evaluated Runx2 as an important marker for osteogenesis in Hippo pathway [51,52]. Runx2 can directly associate with YAP, and its nuclear localization trend resembled that of YAP [53,54]. Nuclear localization intensified in the HBO and HBO + FSS groups (Fig. 4H–J), demonstrating that osteogenic proteins were also increased by HBO and FSS. In summary, the upregulation trends of these three markers on day 14 were not more pronounced compared with those on day 7. However, they appeared to be attenuated. Therefore, we hypothesized that the positive effects of HBO and FSS on osteogenesis primarily occurred during osteogenesis.

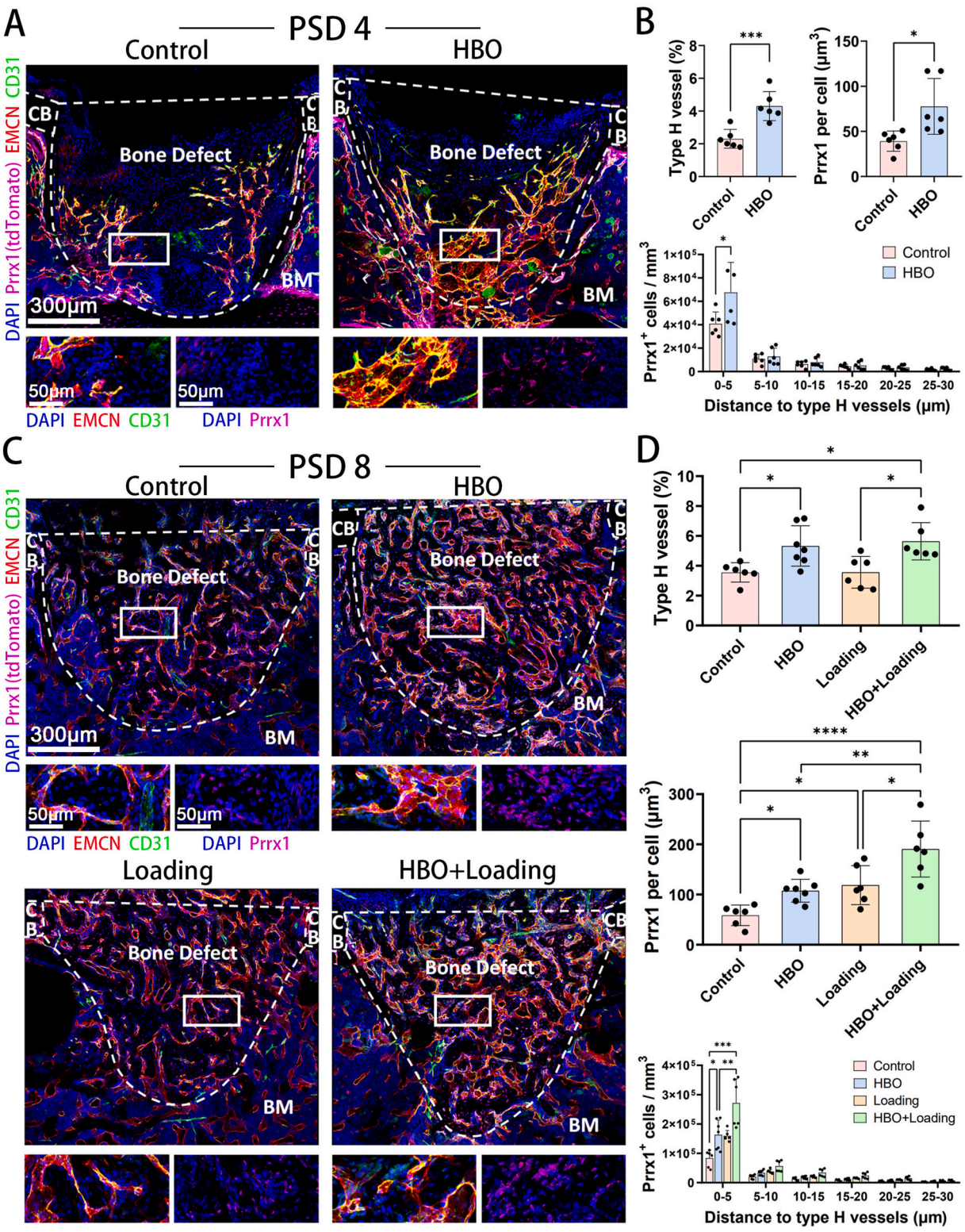

Fig. 2. HBO therapy and mechanical loading promoted angiogenesis, increased number of osteogenic cells. (A–D) Prrx1-expressing (tdTomato^{+}) cells and immunofluorescence staining of endomucin (EMCN, red), CD31 (green), and DAPI (blue) in the cortical bone defect region on (**A**) PSD4 and (**C**) PSD8. CB, cortical bone; BM, bone marrow; zoomed-in images of regions enclosed by solid white lines are shown below. Volume of type H (EMCN^{hi}CD31^{hi}) vessels, volume of Prrx1 per cell, and the number of Prrx1^{+} cells classified by the distance between Prrx1^{+} cells and type H vessels on (**B**) PSD4 and (**D**) PSD8 were analyzed for the whole bone defect region enclosed by dotted white lines; n = 6. Data are means ± SD. *p < 0.05, **p < 0.01, ***p < 0.001, ****p < 0.0001. (For interpretation of the references to color in this figure legend, the reader is referred to the Web version of this article.)

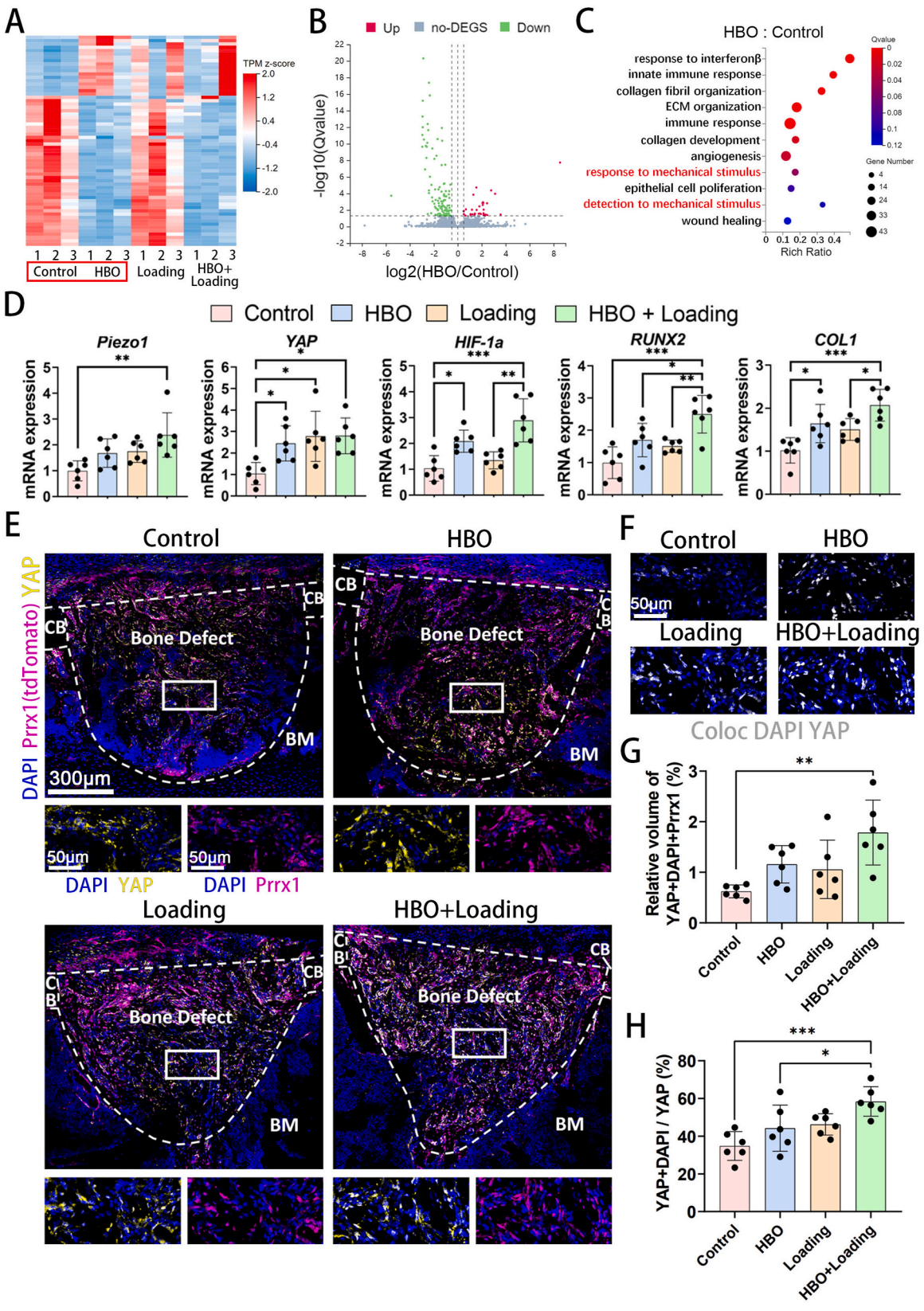

Fig. 3. HBO therapy and mechanical loading stimulated mechanosensitive pathways in bone defects. (A–C) RNA-seq analysis of mRNAs from mouse tibial bone defect tissue on PSD8, including the heatmaps of gene expression (**A**), volcano plot of differential genes induced by HBO (**B**), and gene ontology (GO) enrichment analysis of HBO-induced genes (**C**); n = 3. (**D**) qRT-PCR analysis of mRNAs from mouse tibia bone defect tissue on PSD8; n = 6. (**E**) Prrx1-expressing (tdTomato^{+}) cells and immunofluorescence staining of YAP (yellow) and DAPI (blue) in the cortical bone defect region on PSD8. CB, cortical bone; BM, bone marrow; zoomed-in images of regions enclosed by white lines are shown below. (**F**) Colocalization of YAP and DAPI. (**G**) Volume of nuclear localized YAP in Prrx1^{+} cells on PSD8. The whole bone defect region enclosed by white dotted lines analyzed; n = 6. (**H**) Nuclear localization rate of YAP; n = 6. Data are means ± SD. *p < 0.05, **p < 0.01, ***p < 0.001. (For interpretation of the references to color in this figure legend, the reader is referred to the Web version of this article.)

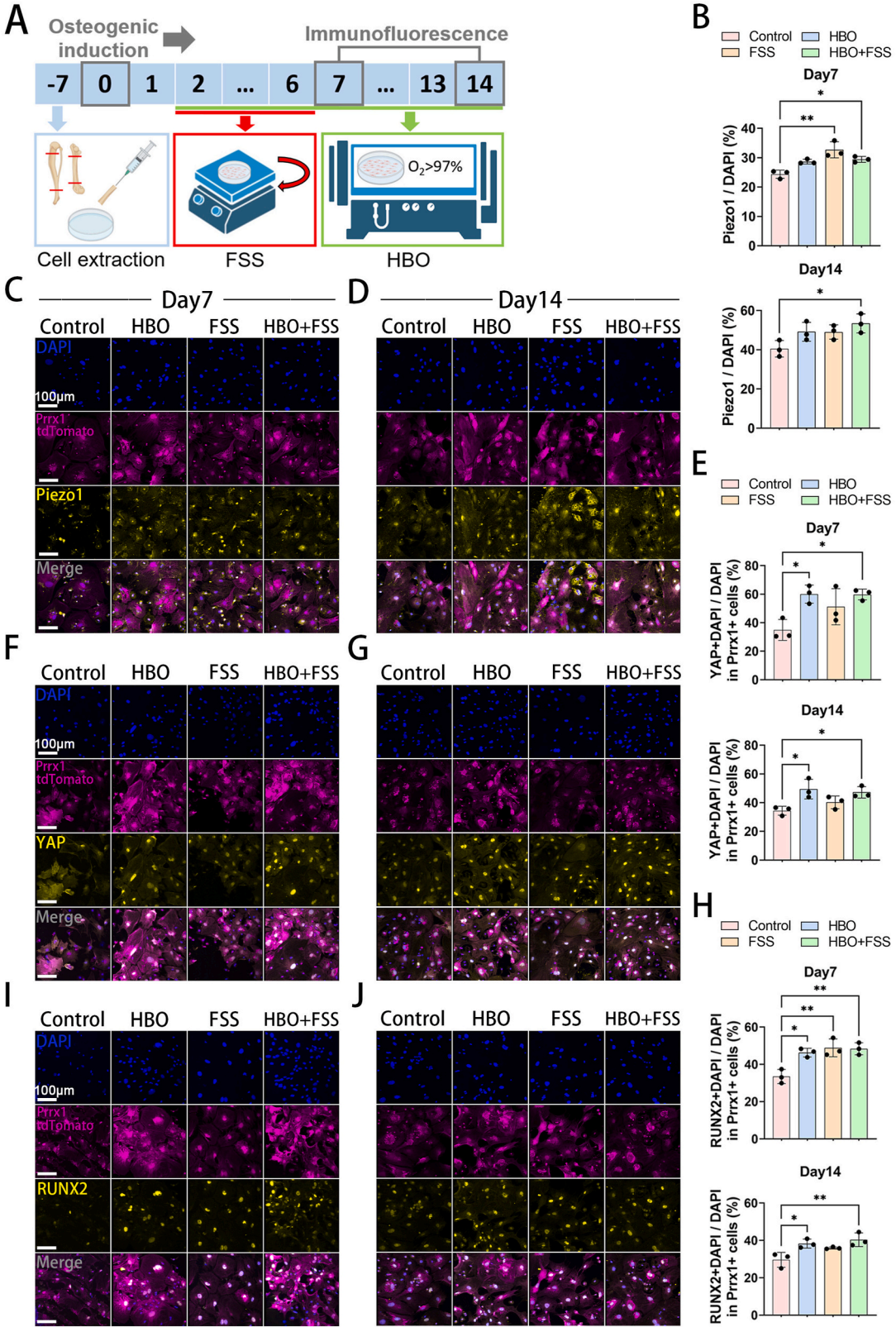

Fig. 4. HBO treatment and mechanical stimulation increased Piezo1 expression, activated YAP and promoted osteogenesis. (**A**) Schematic illustration of the design of in vitro experiments to test the effect of HBO therapy and FSS on osteogenic induction of BMSCs. (**B**–**D**) Prrx1 (tdTomato$^+$) and immunofluorescence staining of Piezo1 (yellow) and DAPI (blue) of BMSCs on (**C**) day 7 and (**D**) day 14 after osteogenic induction. Relative volume of Piezo1 (**B**) was analyzed; n = 3. (**E**–**G**) Prrx1 (tdTomato$^+$) and immunofluorescence staining of YAP (yellow) and DAPI (blue) of BMSCs on (**F**) day 7 and (**G**) day 14 after osteogenic induction. The nuclear localization rate of YAP in Prrx1$^+$ cells (**E**) was analyzed; n = 3. (**H**–**J**) Prrx1 (tdTomato$^+$) and immunofluorescence staining of Runx2 (yellow) and DAPI (blue) of BMSCs on (**I**) day 7 and (**J**) day 14 after osteogenic induction. The nuclear localization rate of Runx2 in Prrx1$^+$ cells (**H**) was analyzed; n = 3. Data are means ± SD. *p < 0.05, **p < 0.01. (For interpretation of the references to color in this figure legend, the reader is referred to the Web version of this article.)

3.5. Conditional knockdown of Piezo1 in Prrx1$^+$ cells abolished the positive effect on bone regeneration induced by HBO therapy or mechanical loading

To determine the role of Piezo1 in promoting bone regeneration during HBO therapy, we knocked out Piezo1 in skeletal stem cells by crossing Piezo1$^{flox/flox}$ mice with Prrx1–Cre transgenic mice. However, homozygous knockout of Piezo1 resulted in poor development and embryonic and postnatal mortality [55], and a significant decrease in skeletal mechanical performance (Fig. S4). Therefore, we employed heterozygous knockout mice and compared them with WT mice. The overall skeletal morphology and volume of type H vessels in bone tissue prior injury did not show significant defference between the two types of mice (Figs. S5–6).

Micro-CT data showed that heterozygous knockout of Piezo1 in Prrx1$^+$ cells abolished the increase in bone volume, BMD, and improvement in bone morphometric properties of bone defect tissues induced by HBO therapy or mechanical loading (Fig. 5A and B). Collagen fiber volume also showed the same absence of response to mechanical loading and HBO in heterogenous knockout animals (Fig. 5C and D). The heterozygous knockout of Piezo1 similarly suppressed the increase in type H vessel volume and Prrx1 protein induced by HBO therapy and mechanical loading (Fig. 5E and F). Spatial correlation analysis revealed that HBO therapy and mechanical loading originally upregulated the number of Prrx1$^+$ cells closest to the type H vessels, but the heterozygous knockout of Piezo1 inhibited this effect (Fig. 5G). Overall, the heterozygous knockout of Piezo1 in skeletal stem cells abolished the positve effects of HBO therapy or mechanical loading on bone regeneration.

3.6. Conditional knockdown of Piezo1 in Prrx1$^+$ cells abolished the activation of the Peizo1–YAP pathway by HBO therapy or mechanical loading

To investigate how the heterozygous knockout of Piezo1 affects bone repair during both treatments, we employed immunofluorescence and qPCR to characterize mechanosensitve pathways associated with Piezo1. Immunofluorescence imaging revealed that the nuclear localization of YAP within the bone defect region did not exhibit significant differences due to HBO therapy or mechanical loading (Fig. 6A and B). Furthermore, the qPCR analysis of mRNA extracted from bone defect tissues revealed that the upregulation of mechanically sensitive genes induced by HBO therapy and mechanical loading was suppressed by the heterozygous knockout of Piezo1 (Fig. 6C). In this process, the combined application of HBO therapy and mechanical loading did not induce a stacking effect, as observed in normal mice. This result indicated that Piezo1 may constitute a shared mechanism through which HBO therapy and mechanical loading promote bone regeneration.

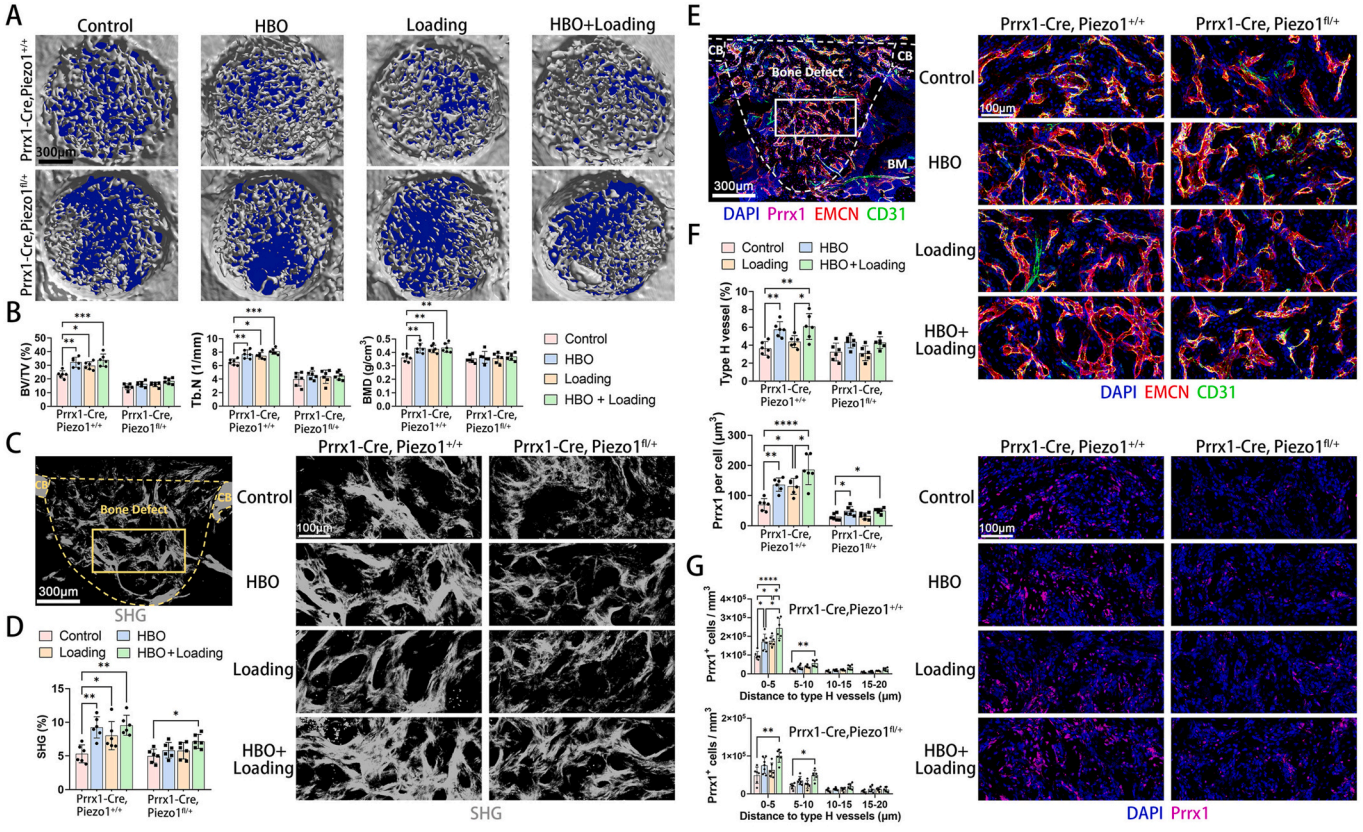

Fig. 5. Knockdown of Piezo1 in Prrx1+ cells abolished the beneficial effect of HBO therapy on osteogenesis and angiogenesis. (**A**) Micro-CT reconstruction of cortical bone defects from Prrx1–Cre, tdTomato mice and Prrx1–Cre, Piezo1$^{fl/+}$ mice on PSD10. (**B**) Bone morphometric properties and BMD of bone-defect regions on PSD10; n = 6. (**C**) SHG signals from collagen fibers in the cortical bone defect region of Prrx1–Cre, tdTomato mice and Prrx1–Cre, Piezo1$^{fl/+}$ mice on PSD8; zoomed-in images of regions enclosed by solid yellow lines are shown on the right. (**D**) Volume of SHG signals on PSD8. The whole bone defect region enclosed by dotted yellow lines analyzed; n = 6. (**E**) Immunofluorescence staining of Prrx1 (purple), endomucin (EMCN, red), CD31 (green), and DAPI (blue) in the cortical bone defect region from Prrx1–Cre, Piezo1$^{fl/+}$ mice on PSD8. CB, cortical bone; BM, bone marrow; zoomed-in images of regions enclosed by solid white lines are shown on the right. (**F–G**) Volume of type H vessels, volume of Prrx1 per cell (**F**), and the number of Prrx1$^+$ cells classified by the distance between Prrx1$^+$ cells and type H vessels (**G**) on PSD8 were analyzed for the whole bone defect region enclosed by dotted white lines; n = 6. Data are means ± SD. *p < 0.05, **p < 0.01, ***p < 0.001, ****p < 0.0001. (For interpretation of the references to color in this figure legend, the reader is referred to the Web version of this article.)

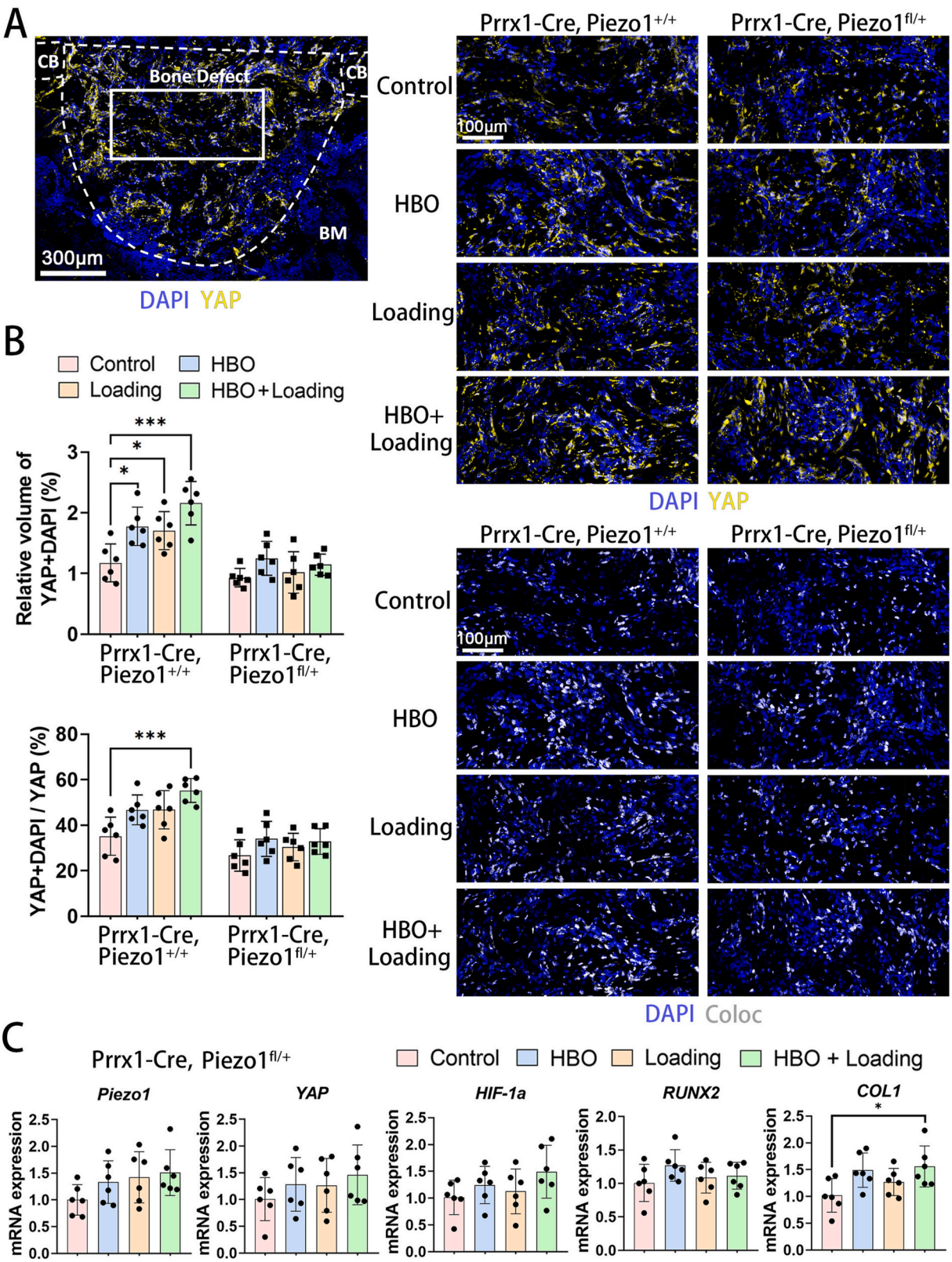

Fig. 6. Knockdown of Piezo1 abolished YAP activation and the increase of mechanosensitive genes caused by HBO therapy. (**A**) Immunofluorescence staining of Prrx1 (purple), YAP (yellow), and DAPI (blue) in the cortical bone defect region of Prrx1–Cre, Piezo1$^{fl/+}$ mice on PSD8. CB, cortical bone; BM, bone marrow; zoomed-in images of regions enclosed by white lines are shown on the right. (**B**) The volume of nuclear localized YAP in Prrx1^{+} cells and nuclear localization rate of YAP on PSD8. The whole bone defect region enclosed by white dotted lines analyzed; n = 6. (**C**) qRT-PCR analysis of mRNAs from Prrx1–Cre, Piezo1$^{fl/+}$ mouse tibia bone defect tissue on PSD8; n = 6. Data are means ± SD. *p < 0.05, **p < 0.01. (For interpretation of the references to color in this figure legend, the reader is referred to the Web version of this article.)

3.7. Conditional knockout and knockdown of Piezo1 reduced HBO-induced and loading-induced osteogenesis in a dose-dependent manner

To further validate the effect of Piezo1 in BMSCs under HBO treatment and mechanical stimulation, we extracted BMSCs from the femurs and tibias of Prrx1–Cre, tdTomato/Prrx1–Cre, Piezo1$^{fl/+}$/Prrx1–Cre, Piezo1$^{fl/fl}$ mice for osteogenic induction (Fig. 7A and S7). A known Piezo1inhibitor GsMTx4 was added to Prrx1–Cre, tdTomato BMSCs as the positive control of Piezo1 inactivation [56,57]. HBO treatment enhanced ALP expression in the BMSCs. The addition of GsMTx4 inhibited the osteogenic-promoting effect of HBO treatment on BMSCs from Prrx1-Cre, tdTomato mice (Fig. 7B and C). We also applied oscillatory FSS to mechanically stimulate the BMSCs from transgenic animals. Furthermore, the heterozygous knockout of Piezo1 in Prrx1^{+} cells suppressed the HBO- and FSS-induced increase in ALP expression, while the magnitude of reduction was even greater in the homozygous knockout of Piezo1 group (Fig. 7D and E).

Alizarin red staining results demonstrated similar reduction in mineralized matrix (Fig. 7F and G). A partial inhibition of Piezo1 expression led to a partial reduction in the stimulatory effects of HBO and mechanical stimulation on osteogenesis. The qPCR results on day 7 revealed that HBO therapy and FSS upregulated the expression of mechanosensitive genes, Piezo1 and YAP. In addition, downstream osteogenesis-related genes, Runx2 and COL1, were also upregulated, consistent with the in vivo findings (Fig. 7H). This trend was similarly attenuated with the dose-dependent knockout of Piezo1.

To determine whether HBO can activate Piezo1, BMSCs were labeled with the calcium indicator Fluo-4 AM in vitro. A known Piezo1 agonist Yoda1 was added as the positive control of Piezo1 activation [58,59]. As expected, Yoda1 elevated calcium fluorescence intensity in the BMSCs of normal mice, followed by a gradual decline. However, this response was reduced in the BMSCs from Prrx1-Cre, Piezo1$^{fl/+}$ and Prrx1–Cre, Piezo1$^{fl/fl}$ mice (Fig. 7I and J). HBO treatment on the cell-culture medium doubled the dissolved oxygen concentration, resulting in a 1.5-fold elevation 60 min after treatment (Fig. S8). The HBO-treated medium increased intracellular calcium influx in the BMSCs of normal mice, while the Piezo1 knockout BMSCs did not respond.

4. Discussion

The nonunion of bones is one of the most common musculoskeletal disorders in clinical practice, and primarily characterized by localized hypoxia that inhibits vascular invasion and bone regeneration [60]. HBO therapy has been employed in various tissue regeneration contexts, such as skin, brain and nerve [5,6]. However, the potential application of HBO therapy in promoting bone tissue regeneration and its underlying biological mechanisms remain unclear. In this study, we sought to determine whether HBO can stimulate bone tissue regeneration through a mechanosensitive pathway, a known regenerative method. Additionally, we assessed the combined effects of HBO therapy and mechanical loading and explored their biological mechanisms.

Our studies first focused on the influence of HBO therapy on bone tissue regeneration. We compared the effects of HBO therapy with those induced by mechanical loading. We found that, HBO therapy promoted bone tissue regeneration, similar to mechanical loading. This effect was evidenced by an increase in bone mass and biomechanical properties at the site of bone defects. Type H vessels, which are crucial vascular components in bone tissue development and regeneration [22,23,61], also exhibited an increase in volume. Additionally, the distance between type H vessels and Prrx1^{+} cells was significantly reduced, suggesting that HBO therapy enhanced the interaction between type H vessels and Prrx1^{+} cells. Furthermore, we discovered that the combined application of HBO therapy and mechanical loading did not result in considerable improvement compared with each treatment alone, indicating that the effects of HBO therapy and mechanical loading on bone repair may have common mechanisms.

The mechanosensitive membrane protein Piezo1 plays an important role in the regulation of bone regeneration in response to mechanical stimulation [46,48,62]. Furthermore, the oxidation of surface membrane lipids increased plasma membrane tension and led to the activation of Piezo1, indicating that elevated oxygen concentrations can activate Piezo1 [39]. Our RNA-seq analysis revealed that HBO treatment promoted the expression of Piezo1, which may explain the similar levels of effects of HBO therapy and mechanical loading on bone tissue regeneration. Therefore, we focused on Piezo1 and studied the role it plays in bone tissue regeneration. qPCR data showed that both HBO or mechanical loading increased Piezo1 expression, and further increase was observed when both treatments were applied. Previous studies have reported that the Piezo1-YAP pathway is a crucial mechanosensory pathway in bone formation. The nuclear translocation of YAP serves as an indicator of the activation of downstream osteogenesis-related genes [38,48]. Through in vivo and in vitro immunofluorescence imaging, we found that the nuclear translocation of YAP in Prrx1^{+} cells was upregulated in response to HBO and mechanical loading. In addition, Runx2, which is a significant downstream transcription factor in the YAP pathway, also increased in both treatment groups, indicating a positive effect on osteogenesis. This result supported our hypothesis that the Piezo1/YAP/Runx2 pathway is one of the essential biological mechanisms through which HBO promotes bone tissue regeneration [37]. Although our study focused on the Piezo1–YAP axis, other mechanosensitive and oxygen-sensitive pathways may play a role in HBO-induced bone formation. Indeed, we observed an upregulation of the hypoxia-inducible factor HIF-1α in the HBO group, consistent with previous findings showing elevated HIF-1α in BMSCs in a high-oxygen environment [63,64]. However, further work is required to determine whether the YAP/HIF-1α pathway constitute a downstream biomechanism influenced by HBO therapy.

Prrx1^{+} cells are considered skeletal stem cells and essential for bone regeneration [27]. The knockout of Piezo1 in Prrx1^{+} cells resulted in reduced bone formation and spontaneous bone fracture in neonatal mice. Our study showed that the homogeneous knockout of Piezo1 in the Prrx1^{+} cells led to similar skeletal malformation, spontaneous fracture, and early death [55]. To study the loss of Piezo1 in adult mice, we employed heterogeneous knockout of Piezo1 in our animal experiments, showing the reduced osteogenic and angiogenic effects promoted by HBO therapy. Furthermore, qPCR data indicated that the upregulation of several osteogenesis-related genes upregulated by HBO was also attenuated. These results suggested a critical role of Piezo1 expression in skeletal stem cells during HBO-induced bone tissue regeneration. In vitro, we utilized Prrx1^{+} cells with homozygous Piezo1 knockout to study the role of Piezo1 in osteogenesis. By comparing cells from homozygous and heterozygous mice, we found a dose-dependent reduction in the stimulatory effects of HBO and mechanical stimulation on osteogenesis after Piezo1 expression was inhibited. Furthermore, we observed that the HBO-treated medium was enriched in oxygen, and it induced intracellular calcium influx through Piezo1 in BMSCs. Thus, elevation in oxygen levels may be one of the mechanisms through which HBO activates Piezo1. Potentially, oxygen can activate Piezo1 by increasing membrane tension through lipid peroxidation [39]. In addition to oxygen, HBO-induced change in hydrostatic pressure in local tissues may be a cause of Piezo1 activation [65], but this relationship requires further investigation.

In summary, our study demonstrated a small animal model of HBO therapy for bone tissue regeneration. Using conditional knockout mice, we discovered that the mechanosensitive Piezo1/YAP/Runx2 pathway is a mechanism through which HBO therapy regulates the osteogenic process. Similar to mechanical loading, which is a known method for promoting bone repair, HBO enhances osteogenesis. The findings provided a mechanism explaining the beneficial effects of HBO therapy on bone regeneration.

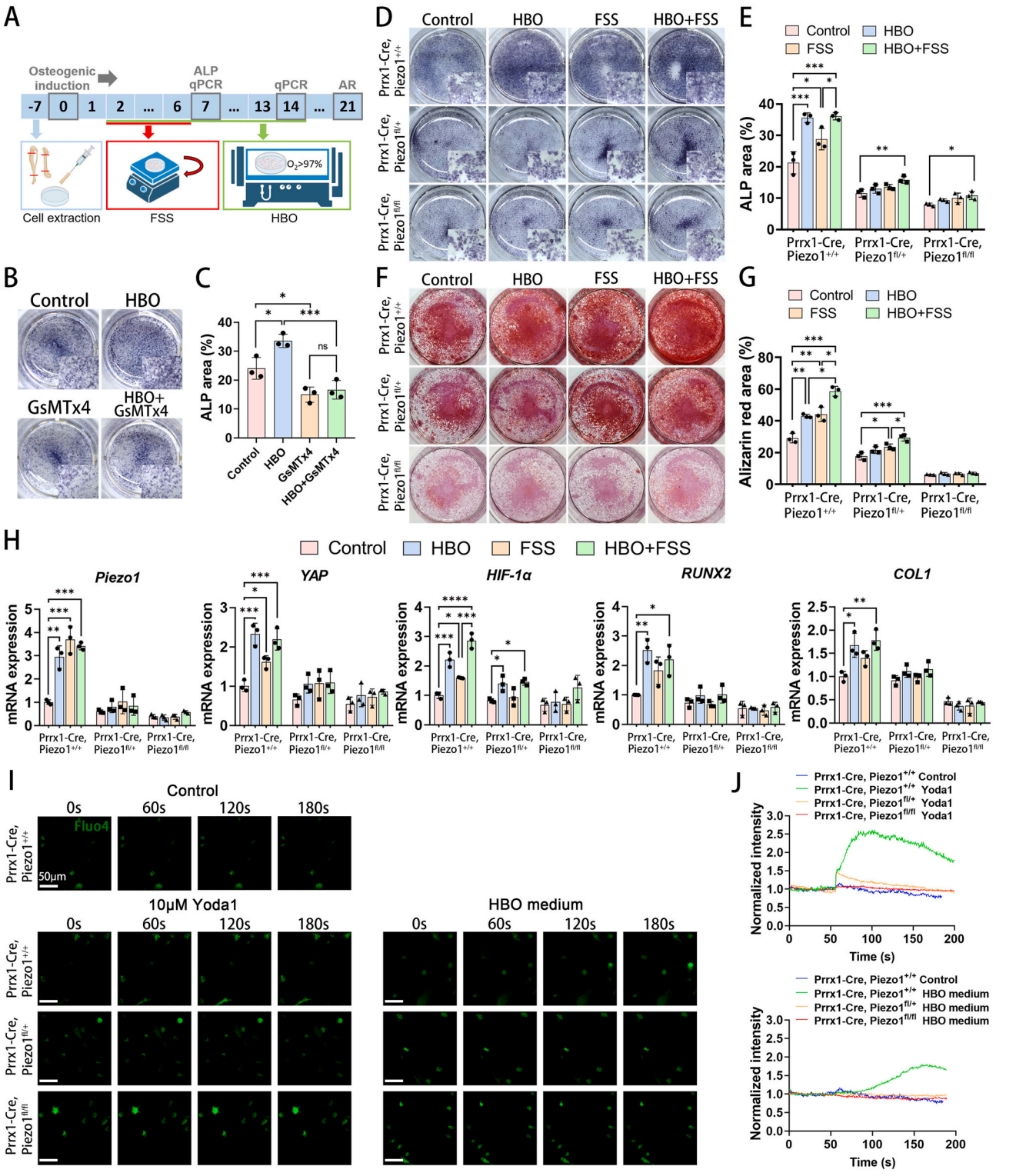

Fig. 7. Conditional knockout and knockdown of Piezo1 led to dose-dependent reduction in the positive effects of HBO and mechanical stimulation on osteogenesis. (**A**) Schematic illustration of the design of in vitro experiments to explore the effect of Piezo1 on osteogenic induction of BMSCs. (**B**) ALP staining and (**C**) analysis of BMSCs from Prrx1–Cre, tdTomato mouse on day 7 after osteogenic induction with the treatment of HBO and GsMTx4; n = 3. (**D**) ALP staining and (**E**) analysis of BMSCs from Prrx1–Cre, tdTomato/Piezo1$^{fl/+}$/Piezo1$^{fl/fl}$ mice on day 7 after osteogenic induction; n = 3. (**F**) Alizarin red staining and (**G**) analysis of BMSCs from Prrx1–Cre, tdTomato/Piezo1$^{fl/+}$/Piezo1$^{fl/fl}$ mice on day 14 after osteogenic induction; n = 3. (**H**) qRT-PCR analysis of mRNAs from BMSCs on day 7; n = 3. (**I**) Fluo4 calcium imaging (488 nm) before and after Yoda1 or HBO medium treatment (at 59s). (**J**) Fluorescence intensity of Fluo4; n = 5. Data are means ± SD. *p < 0.05, **p < 0.01, ***p < 0.001, ****p < 0.0001. (For interpretation of the references to color in this figure legend, the reader is referred to the Web version of this article.)

Author contributions

H.Z., C.L., X.Y. and G.F. designed the research study. H.Z. and C.L. wrote the manuscript. H.Z. performed most of the experiments and analyzed the data. H.L. and M.Li. provided expertise related to the experiments. M.Lin. acquired and analyzed the DIC data. H.W. helped analyze the confocal data. J.Z. conducted the breeding, maintenance, and genotyping of mice.

Declaration of competing interest

The author(s) have no conflicts of interest relevant to this article.

Acknowledgment

Funding for this research was provided by Guangdong Basic and Applied Basic Research Foundation (2021A1515011447), Shenzhen Science and Technology Innovation Commission (KQTD20200820113012029), and the Guangdong Provincial Key Laboratory of Advanced Biomaterials (2022B1212010003). A portion of the confocal data were obtained using equipment maintained by Southern University of Science and Technology Core Research Facilities.

Appendix A. Supplementary data

Supplementary data to this article can be found online at https://doi.org/10.1016/j.jot.2024.07.001.

References

[1] Huang C, Zhong Y, Yue C, He B, Li Y, Li J. The effect of hyperbaric oxygen therapy on the clinical outcomes of necrotizing soft tissue infections: a systematic review and meta-analysis. World J Emerg Surg 2023;18(1):23.
[2] Leach RM, Rees PJ, Wilmshurst P. Hyperbaric oxygen therapy. BMJ 1998;317(7166):1140–3.
[3] Borromeo CN, Ryan JL, Marchetto PA, Peterson R, Bove AA. Hyperbaric oxygen therapy for acute ankle sprains. Am J Sports Med 1997;25(5):619–25.
[4] Oyaizu T, Enomoto M, Yamamoto N, Tsuji K, Horie M, Muneta T, et al. Hyperbaric oxygen reduces inflammation, oxygenates injured muscle, and regenerates skeletal muscle via macrophage and satellite cell activation. Sci Rep 2018;8(1):1288.
[5] Fischer BH. Topical hyperbaric oxygen treatment of pressure sores and skin ulcers. Lancet 1969;2(7617):405–9.
[6] Camporesi EM, Vezzani G, Bosco G, Mangar D, Bernasek TL. Hyperbaric oxygen therapy in femoral head necrosis. J Arthroplasty 2010;25(6 Suppl):118–23.
[7] Yamamoto N, Oyaizu T, Enomoto M, Horie M, Yuasa M, Okawa A, et al. VEGF and bFGF induction by nitric oxide is associated with hyperbaric oxygen-induced angiogenesis and muscle regeneration. Sci Rep 2020;10(1):2744.
[8] Juskovic A, Nikolic M, Ljujic B, Matic A, Zivkovic V, Vucicevic K, et al. Effects of combined allogenic adipose stem cells and hyperbaric oxygenation treatment on pathogenesis of osteoarthritis in knee joint induced by monoiodoacetate. Int J Mol Sci 2022;23(14).
[9] Kessler L, Bilbault P, Ortega F, Grasso C, Passemard R, Stephan D, et al. Hyperbaric oxygenation accelerates the healing rate of nonischemic chronic diabetic foot ulcers: a prospective randomized study. Diabetes Care 2003;26(8):2378–82.
[10] Burge R, Dawson-Hughes B, Solomon DH, Wong JB, King A, Tosteson A. Incidence and economic burden of osteoporosis-related fractures in the United States, 2005-2025. J Bone Miner Res 2007;22(3):465–75.
[11] Boerckel JD, Uhrig BA, Willett NJ, Huebsch N, Guldberg RE. Mechanical regulation of vascular growth and tissue regeneration in vivo. Proc Natl Acad Sci U S A 2011;108(37):E674–80.
[12] Liu C, Cabahug-Zuckerman P, Stubbs C, Pendola M, Cai C, Mann KA, et al. Mechanical loading promotes the expansion of primitive osteoprogenitors and organizes matrix and vascular morphology in long bone defects. J Bone Miner Res 2019;34(5):896–910.
[13] Zhang J, Tong Y, Liu Y, Lin M, Xiao Y, Liu C. Mechanical loading attenuated negative effects of nucleotide analogue reverse-transcriptase inhibitor TDF on bone repair via Wnt/beta-catenin pathway. Bone 2022;161:116449.
[14] Zhu C, Lin J, Jiang H, Gao J, Gao M, Wu B, et al. Combination of optimized tissue engineering bone implantation with heel-strike like mechanical loading to repair segmental bone defect in New Zealand rabbits. Cell Tissue Res 2021;385(3):639–58.
[15] Youngstrom DW, Senos R, Zondervan RL, Brodeur JD, Lints AR, Young DR, et al. Intraoperative delivery of the Notch ligand Jagged-1 regenerates appendicular and craniofacial bone defects. NPJ Regen Med 2017;2:32.
[16] Liu Y, Zhu Z, Pei X, Zhang X, Cheng X, Hu S, et al. ZIF-8-Modified multifunctional bone-adhesive hydrogels promoting angiogenesis and osteogenesis for bone regeneration. ACS Appl Mater Interfaces 2020;12(33):36978–95.
[17] Pandya M, Saxon M, Bozanich J, Tillberg C, Luan X, Diekwisch TGH. The glycoprotein/cytokine erythropoietin promotes rapid alveolar ridge regeneration in vivo by promoting new bone extracellular matrix deposition in conjunction with coupled angiogenesis/osteogenesis. Int J Mol Sci 2021;22(6).
[18] Kan T, He Z, Du J, Xu M, Cui J, Han X, et al. Irisin promotes fracture healing by improving osteogenesis and angiogenesis. J Orthop Translat 2022;37:37–45.
[19] Liao F, Liao Z, Zhang T, Jiang W, Zhu P, Zhao Z, et al. ECFC-derived exosomal THBS1 mediates angiogenesis and osteogenesis in distraction osteogenesis via the PI3K/AKT/ERK pathway. J Orthop Translat 2022;37:12–22.
[20] Herath SC, Lion T, Klein M, Stenger D, Scheuer C, Holstein JH, et al. Stimulation of angiogenesis by cilostazol accelerates fracture healing in mice. J Orthop Res 2015;33(12):1880–7.
[21] Hausman MR, Schaffler MB, Majeska RJ. Prevention of fracture healing in rats by an inhibitor of angiogenesis. Bone 2001;29(6):560–4.
[22] Kusumbe AP, Ramasamy SK, Adams RH. Coupling of angiogenesis and osteogenesis by a specific vessel subtype in bone. Nature 2014;507(7492):323–8.
[23] Wang L, Zhou F, Zhang P, Wang H, Qu Z, Jia P, et al. Human type H vessels are a sensitive biomarker of bone mass. Cell Death Dis 2017;8(5):e2760.
[24] Ramasamy SK, Kusumbe AP, Itkin T, Gur-Cohen S, Lapidot T, Adams RH. Regulation of hematopoiesis and osteogenesis by blood vessel-derived signals. Annu Rev Cell Dev Biol 2016;32:649–75.
[25] Wang X, Li X, Li J, Zhai L, Liu D, Abdurahman A, et al. Mechanical loading stimulates bone angiogenesis through enhancing type H vessel formation and downregulating exosomal miR-214-3p from bone marrow-derived mesenchymal stem cells. Faseb J 2021;35(1):e21150.
[26] Yang C, Liu Y, Wang Z, Lin M, Liu C. Controlled mechanical loading improves bone regeneration by regulating type H vessels in a S1Pr1-dependent manner. Faseb J 2022;36(10):e22530.
[27] Liu H, Li P, Zhang S, Xiang J, Yang R, Liu J, et al. Prrx1 marks stem cells for bone, white adipose tissue and dermis in adult mice. Nat Genet 2022;54(12):1946–58.
[28] Xiao H, Zhang T, Li C, Cao Y, Wang L, Chen H, et al. Mechanical stimulation promotes enthesis injury repair by mobilizing Prrx1(+) cells via ciliary TGF-beta signaling. Elife 2022;11.
[29] Zhang K, Qiu W, Li H, Li J, Wang P, Chen Z, et al. MACF1 overexpression in BMSCs alleviates senile osteoporosis in mice through TCF4/miR-335-5p signaling pathway. J Orthop Translat 2023;39:177–90.
[30] Sun X, Li X, Qi H, Hou X, Zhao J, Yuan X, et al. MiR-21 nanocapsules promote early bone repair of osteoporotic fractures by stimulating the osteogenic differentiation of bone marrow mesenchymal stem cells. J Orthop Translat 2020;24:76–87.
[31] Wilk K, Yeh SA, Mortensen LJ, Ghaffarigarakani S, Lombardo CM, Bassir SH, et al. Postnatal calvarial skeletal stem cells expressing PRX1 reside exclusively in the calvarial sutures and are required for bone regeneration. Stem Cell Rep 2017;8(4):933–46.
[32] Moore ER, Zhu YX, Ryu HS, Jacobs CR. Periosteal progenitors contribute to load-induced bone formation in adult mice and require primary cilia to sense mechanical stimulation. Stem Cell Res Ther 2018;9(1):190.
[33] Coste B, Mathur J, Schmidt M, Earley TJ, Ranade S, Petrus MJ, et al. Piezo1 and Piezo2 are essential components of distinct mechanically activated cation channels. Science 2010;330(6000):55–60.
[34] Lin YC, Guo YR, Miyagi A, Levring J, MacKinnon R, Scheuring S. Force-induced conformational changes in PIEZO1. Nature 2019;573(7773):230–4.
[35] Chen S, Li Z, Chen D, Cui H, Wang J, Li Z, et al. Piezo1-mediated mechanotransduction promotes entheseal pathological new bone formation in ankylosing spondylitis. Ann Rheum Dis 2023;82(4):533–45.
[36] Zhang G, Li X, Wu L, Qin YX. Piezo1 channel activation in response to mechanobiological acoustic radiation force in osteoblastic cells. Bone Res 2021;9(1):16.
[37] Zhong G, Su S, Li J, Zhao H, Hu D, Chen J, et al. Activation of Piezo1 promotes osteogenic differentiation of aortic valve interstitial cell through YAP-dependent glutaminolysis. Sci Adv 2023;9(22):eadg0478.
[38] Liu Y, Tian H, Hu Y, Cao Y, Song H, Lan S, et al. Mechanosensitive Piezo1 is crucial for periosteal stem cell-mediated fracture healing. Int J Biol Sci 2022;18(10):3961–80.
[39] Hirata Y, Cai R, Volchuk A, Steinberg BE, Saito Y, Matsuzawa A, et al. Lipid peroxidation increases membrane tension, Piezo1 gating, and cation permeability to execute ferroptosis. Curr Biol 2023;33(7):1282–12894 e5.
[40] Bouxsein ML, Boyd SK, Christiansen BA, Guldberg RE, Jepsen KJ, Muller R. Guidelines for assessment of bone microstructure in rodents using micro-computed tomography. J Bone Miner Res 2010;25(7):1468–86.
[41] Thompson MS, Schell H, Lienau J, Duda GN. Digital image correlation: a technique for determining local mechanical conditions within early bone callus. Med Eng Phys 2007;29(7):820–3.
[42] Kusumbe AP, Ramasamy SK, Starsichova A, Adams RH. Sample preparation for high-resolution 3D confocal imaging of mouse skeletal tissue. Nat Protoc 2015;10(12):1904–14.
[43] Mangan AP, Whitaker RT. Partitioning 3D surface meshes using watershed segmentation. IEEE Trans Visual Comput Graph 1999;5(4):308–21.
[44] Soleimani M, Nadri S. A protocol for isolation and culture of mesenchymal stem cells from mouse bone marrow. Nat Protoc 2009;4(1):102–6.
[45] Nair A, Chuang SC, Lin YS, Chen CH, Fang TC, Chiu HC, et al. Characterization of collagen response to bone fracture healing using polarization-SHG. Sci Rep 2022;12(1):18453.
[46] Li X, Han L, Nookaew I, Mannen E, Silva MJ, Almeida M, et al. Stimulation of Piezo1 by mechanical signals promotes bone anabolism. Elife 2019;8.
[47] Dupont S, Morsut L, Aragona M, Enzo E, Giulitti S, Cordenonsi M, et al. Role of YAP/TAZ in mechanotransduction. Nature 2011;474(7350):179–83.

[48] Wang L, You X, Lotinun S, Zhang L, Wu N, Zou W. Mechanical sensing protein PIEZO1 regulates bone homeostasis via osteoblast-osteoclast crosstalk. Nat Commun 2020;11(1):282.
[49] Du J, Yang J, He Z, Cui J, Yang Y, Xu M, et al. Osteoblast and osteoclast activity affect bone remodeling upon regulation by mechanical loading-induced leukemia inhibitory factor expression in osteocytes. Front Mol Biosci 2020;7:585056.
[50] Pei T, Su G, Yang J, Gao W, Yang X, Zhang Y, et al. Fluid shear stress regulates osteogenic differentiation via AnnexinA6-mediated autophagy in MC3T3-E1 cells. Int J Mol Sci 2022;23(24).
[51] Perez-Campo FM, Santurtun A, Garcia-Ibarbia C, Pascual MA, Valero C, Garces C, et al. Osterix and RUNX2 are transcriptional regulators of sclerostin in human bone. Calcif Tissue Int 2016;99(3):302–9.
[52] Suo J, Feng X, Li J, Wang J, Wang Z, Zhang L, et al. VGLL4 promotes osteoblast differentiation by antagonizing TEADs-inhibited Runx2 transcription. Sci Adv 2020;6(43).
[53] Zhao X, Tang L, Le TP, Nguyen BH, Chen W, Zheng M, et al. Yap and Taz promote osteogenesis and prevent chondrogenesis in neural crest cells in vitro and in vivo. Sci Signal 2022;15(757):eabn9009.
[54] Xiong J, Almeida M, O'Brien CA. The YAP/TAZ transcriptional co-activators have opposing effects at different stages of osteoblast differentiation. Bone 2018;112:1–9.
[55] Zhou T, Gao B, Fan Y, Liu Y, Feng S, Cong Q, et al. Piezo1/2 mediate mechanotransduction essential for bone formation through concerted activation of NFAT-YAP1-ss-catenin. Elife 2020;9.
[56] Ren X, Zhuang H, Li B, Jiang F, Zhang Y, Zhou P. Gsmtx4 alleviated osteoarthritis through piezo1/calcineurin/NFAT1 signaling Axis under excessive mechanical strain. Int J Mol Sci 2023;24(4).
[57] Gnanasambandam R, Ghatak C, Yasmann A, Nishizawa K, Sachs F, Ladokhin AS, et al. GsMTx4: mechanism of inhibiting mechanosensitive ion channels. Biophys J 2017;112(1):31–45.
[58] Botello-Smith WM, Jiang W, Zhang H, Ozkan AD, Lin YC, Pham CN, et al. A mechanism for the activation of the mechanosensitive Piezo1 channel by the small molecule Yoda1. Nat Commun 2019;10(1):4503.
[59] Wijerathne TD, Ozkan AD, Lacroix JJ. Yoda1's energetic footprint on Piezo1 channels and its modulation by voltage and temperature. Proc Natl Acad Sci U S A 2022;119(29):e2202269119.
[60] Zura R, Xiong Z, Einhorn T, Watson JT, Ostrum RF, Prayson MJ, et al. Epidemiology of fracture nonunion in 18 human bones. JAMA Surg 2016;151(11):e162775.
[61] Zhang T, Yan S, Song Y, Chen C, Xu D, Lu B, et al. Exosomes secreted by hypoxia-stimulated bone-marrow mesenchymal stem cells promote grafted tendon-bone tunnel healing in rat anterior cruciate ligament reconstruction model. J Orthop Translat 2022;36:152–63.
[62] Sun W, Chi S, Li Y, Ling S, Tan Y, Xu Y, et al. The mechanosensitive Piezo1 channel is required for bone formation. Elife 2019;8.
[63] Kim HS, Ha HS, Kim DH, Son DH, Baek S, Park J, et al. O(2) variant chip to simulate site-specific skeletogenesis from hypoxic bone marrow. Sci Adv 2023;9(12):eadd4210.
[64] Salhanick SD, Belikoff B, Orlow D, Holt D, Reenstra W, Buras JA. Hyperbaric oxygen reduces acetaminophen toxicity and increases HIF-1alpha expression. Acad Emerg Med 2006;13(7):707–14.
[65] Kurbel S, Curkovic V, Kovacic B. Hypothesis: drainage of the peripheral tissue edema by the hyperbaric oxygen therapy because of hyperoxygenation that constricts arterioles and alters the downstream capillary fluid traffic in affected tissues. Bioessays 2023;45(6):e2300023.